Supporting information

Metal Boride Better Than Pt: HCP Pd₂B as Superactive Hydrogen Evolution Reaction Catalyst

Lin Chen,[a] Ling-Ran Zhang,[b] Ling-Yan Yao,[c] Ya-Hui Fang,[c] Lin He,[d] Guang-Feng Wei[*b] and Zhi-Pan Liu[*a]

[a] Collaborative Innovation Center of Chemistry for Energy Material, Shanghai Key Laboratory of Molecular Catalysis and Innovative Materials, Key Laboratory of Computational Physical Science, Department of Chemistry, Fudan University, Shanghai 200433, China

[b] Shanghai Key Laboratory of Chemical Assessment and Sustainability, State Key Laboratory of Pollution Control and Resources Reuse, School of Chemical Science and Engineering, Tongji University, Shanghai 200092, China.

[c] School of Chemical and Environmental Engineering, Shanghai Institute of Technology, Shanghai, 201418, China

[d] Lanzhou Institute of Chemical Physics (LICP), Chinese Academy of Sciences Lanzhou 730000, China

Contents

1. Experimental methods and calculation details

Materials used: Palladium(II) 2,4-pentanedionate ((Pd(acac)$_2$, Pd 34.7%), Sodium palladium(II) chloride (Na$_2$PdCl$_4$, Pd 36.1%), L-ascorbic acid (AA, 99+%), Polyvinylpyrrolidone (PVP, 41631), Borane-tetrahydrofuran complex, (BH$_3$–THF, 1 M solution in THF), dimethylamine borane (DMAB, Me$_2$NH·BH$_3$), and Nafion (D-520 dispersion, 5% w/w in water and 1-propanol) were obtained from Alfa Aesar. Commerical Pt/C(20%), PVP (MW ≈ 30 000), KBr (99%), Cetyltrimethylammonium bromide (CTAB, >99.0%), 2-phenylethanol (>98.0%) were purchased from Sigma Aldrich., Ethanol (99.7%), Tetrahydrofuran (99.9%, anhydrous), Acetone (99.5%), Nitric acid (65 ~ 68%) and Sulfuric acid (95–98%) were purchased from Sinopharm Chemical Reagent Co., Ltd. Vulcan XC-72R carbon (C) was purchased from Cabot Corporation (USA). All the chemicals were used directly without further purification. N$_2$ (oxygen free compressed nitrogen), H$_2$ (99.99%) and CO (Carbon monoxide CP grade 99.9%) was supplied by Shanghai Tomoe gases Co., Ltd. All aqueous solutions were prepared using deionized (DI) water with a resistivity of 18.2 MΩ cm.

Characterization methods: The morphologies of the samples were characterized by field emission scanning electron microscopy (FESEM, Hitachi, S-4800, Japan). Transmission electron microscopy (TEM) images were taken using a Tecnai G2 F20 S-Twin (FEI, USA). X-ray photoelectron spectroscopy (XPS) was conducted on Perkin-Elmer PHI 5000C ESCA system using a Mg Ka (hν =1253.6 eV) radiation source. Ultraviolet photoelectron spectroscopy (UPS) was performed using a He I (21.22 eV) UV source (AXIS Ultra DLD, Kratos, Japan). The X-ray diffraction (XRD) study was carried out using Bruker D8 Advance (Cu Kα radiation, Bruker AXS, Germany). Magnetic susceptibility was measured using a SQUID–VSM (SVSM, Quantum Design, USA).

Synthesis of Pd nanosheets supported on Vulcan XC-72R carbon (Pd NS/C): Briefly, 50 mL of 2-phenylethanol containing PVP (MW ≈ 30 000, 960 mg), CTAB (185 mg) and Vulcan XC-72R carbon (104.1 mg) were placed in a 100 mL round-bottomed flask under an atmosphere of CO (100 mL/min) at 100 °C for 10 min with magnetic stirring. Then, 10 mL of 2-phenylethanol containing Pd(acac)$_2$ (300 mg) was added rapidly. The reaction was allowed

to proceed at 100 °C for 3 h under an atmosphere of CO. The products were precipitated by acetone, separated via centrifugation and further purified by an ethanol-acetone mixture. It is also possible to synthesize Pd NS if Vulcan XC-72R carbon is not added in the above synthesis, which has been utilized to understand the role of C in the B insertion process (also see SI Fig. 16)

Synthesis of Pd$_x$B and Pd$_2$B NS/C: 30 mg Pd NS/C and excessive amount of dimethylamine borane (DMAB, Me$_2$NH·BH$_3$, 295 mg) and 5 mL THF into a sealed 10 ml Teflon-lined stainless autoclave, continuous stirring and reaction 2 h for various temperatures (70, 90 and 120 ^{o}C). After cooled down naturally to room temperature, the product should be filtered, subsequently washed by THF and ethanol several times, and then dried at 30 °C in vacuum-dried for 12 h. It should be mentioned that we can also successfully obtain the hcp Pd$_2$B nanosheets without adding Vulcan XC-72R carbon. This is evident by the XRD results for the sample prepared without carbon, as shown in Fig. S16.

Synthesis of PVP coated Pd nanocubes (Pd NC@PVP): Here the Pd NC@PVP were synthesized as the precursor of previously reported Pd$_2$B NC@PVP.[1] In a typical synthesis of Pd nanocubes, 80 mL of an aqueous solution containing PVP (Alfa,1.05 g), AA (600 mg), and KBr (300 mg) were placed in a 150 mL round-bottomed flask, and pre-heated in air under magnetic stirring at 80 °C for 10 min. Then, 30 mL of an aqueous solution containing Na$_2$PdCl$_4$ (570 mg) was added rapidly. The reaction was allowed to proceed at 80 °C for 3 h. The product was collected by centrifugation and washed 3 times with water to remove excess PVP.

Synthesis of Pd$_2$B NC@PVP: 30 mg Pd NC@PVP and 10 mL BH$_3$–THF into a sealed 15 ml Teflon-lined stainless autoclave, heated up to 150 °C and continuous stirring for 72 h. The product was collected by centrifugation and washed 3 times with THF and ethanol.

Preparation of the working electrodes: A catalyst slurry was first prepared by mixing 95 µL DI water, 95 µL ethanol and 10 µL nafion (5 wt %), 1.0 mg of catalyst ultrasonically for 40 min. A glassy-carbon electrode (GCE) was polished with 0.05 mm alumina slurry on a Buehler micro polishing cloth. The catalyst ink modified GCE was prepared by drop-casting 5 µL of

the solution on a GCE of diameter 3 mm and drying at ambient temperature in air.

Electrochemical Measurement: All the electrochemical measurements were carried out by using a CHI 660E electrochemical workstation (CH Instruments, Inc). In the conventional three-electrode system, glasscarbon electrode (GCE) was used as the working electrode (the diameter of GCE: 3 mm). A saturated calomel electrode (SCE, saturated KCl) and a carbon rod were applied as the reference electrode and the counter electrode, respectively. The electrocatalytic activity of catalyst towards HER was examined by obtaining polarization curves using linear sweep voltammetry (LSV) at a scan rate of 1 mV s^{-1} at room temperature in N_2-saturated 0.5 M H_2SO_4 solutions. Unless special mention, all data were reported with iR compensation.

CO stripping: Electrochemically active surface area (ECSA) was calculated by CO stripping experiment, first the CV was carried out in 0.5 M H_2SO_4 solution saturated with N_2 at a scan rate of 100 mV s^{-1} within the potential range from 0.05 to 1.35 V ten cycles. And by bubbling CO at 0.25 V for 15 min, then by removing the dissolved CO by bubbling N_2 for 30 min while holding at 0.25 V. At last, the CO stripping was carried out in the potential range from 0.05 to 1.35 V at a scan rate of 10 mV s^{-1}.The ECSA of Pd and Pt/C catalysts were calculated from the following equation：

$$ECSA = Q / (m·C)$$

where Q was the charge in the CO adsorption oxidation region, m was the loading amount of Pt and Pd metal, and C (420 μC cm^{-2}) was the charge required for monolayer adsorption of CO on Pt and Pd surface.

Accelerated degradation tests: To evaluate the durability of the Pd_2B NS/C catalysts for the HER activity, accelerated degradation tests is done by measuring the HER after repeated cycling in the range from 50 mV to -65 mV vs. the RHE for 1000 cycles in 0.5 M H_2SO_4 at a scan rate of 100 mV s^{-1}.

Accelerated Life Test: For a good electrode, it can work effectively for several years under normal conditions, thus it would be time-consuming to test electrode stability. To reduce the

test time, the accelerated life test described below was used to assess electrode stability. A rough evaluation could be made using the method proposed by Hine and co-workers[2], where a simple relationship between the electrode service life (SL) and the current density (i) could be obtained:

$$SL \sim 1/i^n$$

where n ranges from 1.4 to 2.0. It is noted that the real lifetime of the electrode would rely on the test conditions, including current density, pH and temperature of the electrolyte. The tests were carried out in 0.5 M H_2SO_4, at 500 mA cm-2; in these experiments, cathode were considered as passivated upon a 2.2 V increase of their potential under the applied current density. The test was conducted at a constant anodic current density.

Calculation Details: All DFT calculations were performed using VASP packages[3] with projected augmented wave (PAW) pseudo-potentials[4,5]. The exchange–correlation energy was treated based on the generalized gradient approximation (GGA) by using Perdew–Burke–Ernzerhof (PBE) functional[6]. The plane-wave cutoff energy was set to 400 eV. The Monkhorst–Pack scheme with a k-point separation length 0.04 $Å^{-1}$ was utilized for sampling the first Brillion zone. The crystal structures of Pd borides were obtained via the large scale global structure search, which have been introduced in our recent work[7]. Transition states (TSs) of the B transition were searched using the Constrained-Broyden-based TS-searching methods[8,9] and the Double-Ended Surface Walking (DESW) method[10]. Liu group has implemented these TS searching methods and the global optimization methods in a neural-network computing program (LASP www.lasphub.com). LASP can interface with VASP for all the functionalities. For the investigation of B diffusion, we mainly utilized $(2 \times 2\sqrt{3})$ (8 Pd atoms per layer) six-layer slabs with adsorbates on one sides of the (111) surfaces. The bottom two layers in the six-layer slab were held at the bulk truncated position and the other layers were fully relaxed. The same sized Pd(111) and Pd_2B(001) slabs were utilized during the investigation of HER kinetics. The Quasi-Newton l-BFGS method is used for geometry relaxation until the maximal force on each degree of freedom is less than 0.05 eV/Å.

To derive the energy reaction profile, we first obtain the reaction energy of each step

(strictly speaking, Helmholtz free energy change (ΔF) at 0 K, 0 bar) that is directly available from DFT total energy (ΔE) after the ZPE correction. For elementary surface reactions without involving the adsorption/desorption of gaseous molecules, ΔF at 0 K, 0 bar is a good approximation to the Gibbs free energy (ΔG) as the temperature T and pressure p contributions at the solid phase are small. To compute the free energy change ΔG of elementary reactions involving gaseous hydrogen, the large entropy term at 298 K is essential to take into account. We utilize the standard thermodynamic data[11] to obtain the temperature and pressure contributions for the G of the gaseous H_2, which is -0.31 eV compared to the total energy of the corresponding free molecule (E, 0 K), respectively.[12] For reactions involving the proton and electron, the reaction energy can be computed by referencing to the normal hydrogen electrode (NHE) in a manner proposed by the Bockris[13] and Nørskov group[14]. This is governed by $G_{proton+electron} = G(\frac{1}{2}H_2) - neU$ where e presents the transfer electron, n means the number of electrons, and U is the electrochemical potential vs NHE.

2. The SEM, TEM images of Pd NS/C
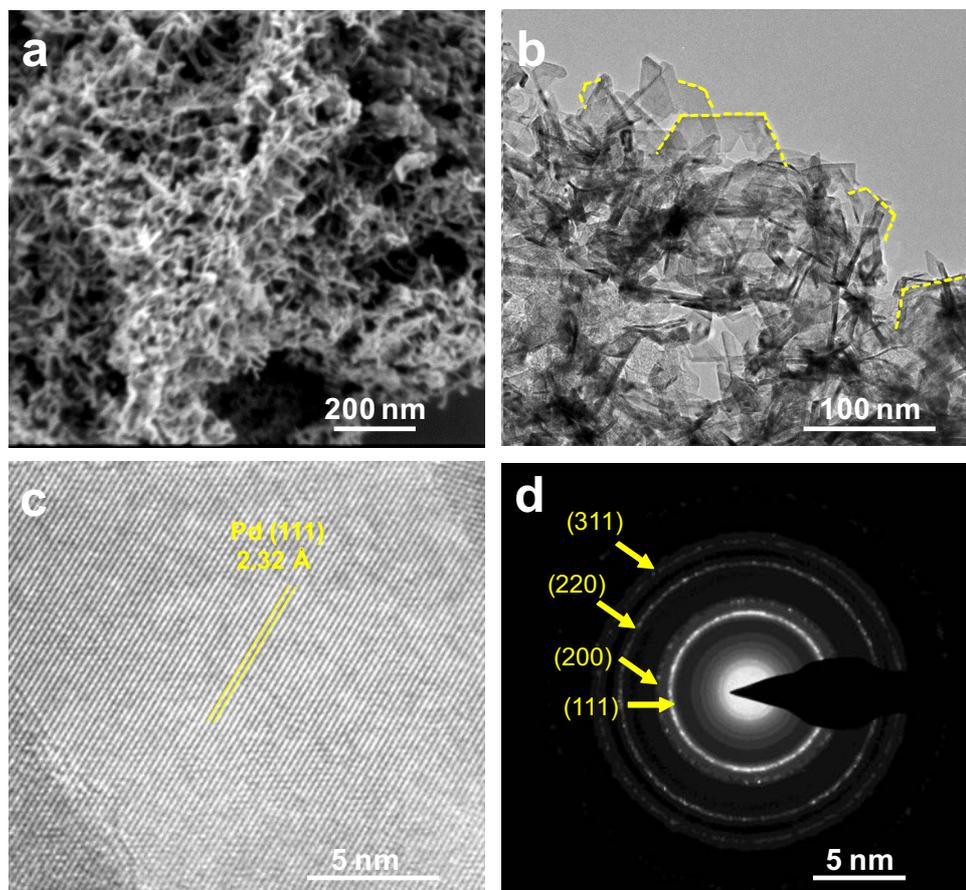
Fig. S1. (a) Scanning electron microscopy (SEM), (b) TEM, (c) HR-TEM and (d) electron diffraction pattern images for Pd NS/C.

Figure S1a-b shows a SEM and TEM image of Pd NS/C, which Pd NS on C are not uniform and range from tens of nanometers to one hundred nanometers. And Figure S1c shows a HR-TEM image of an individual Pd NS that lays flat. The fringes with a lattice spacing of 0.232 nm can be indexed to the (111) planes of Pd with a fcc structure. The electron diffraction pattern corresponds to the (111), (200), (220) and (311) planes of the expected *fcc* Pd (Figure S1d).

3. TEM and HER test of Pd₂B NC@PVP
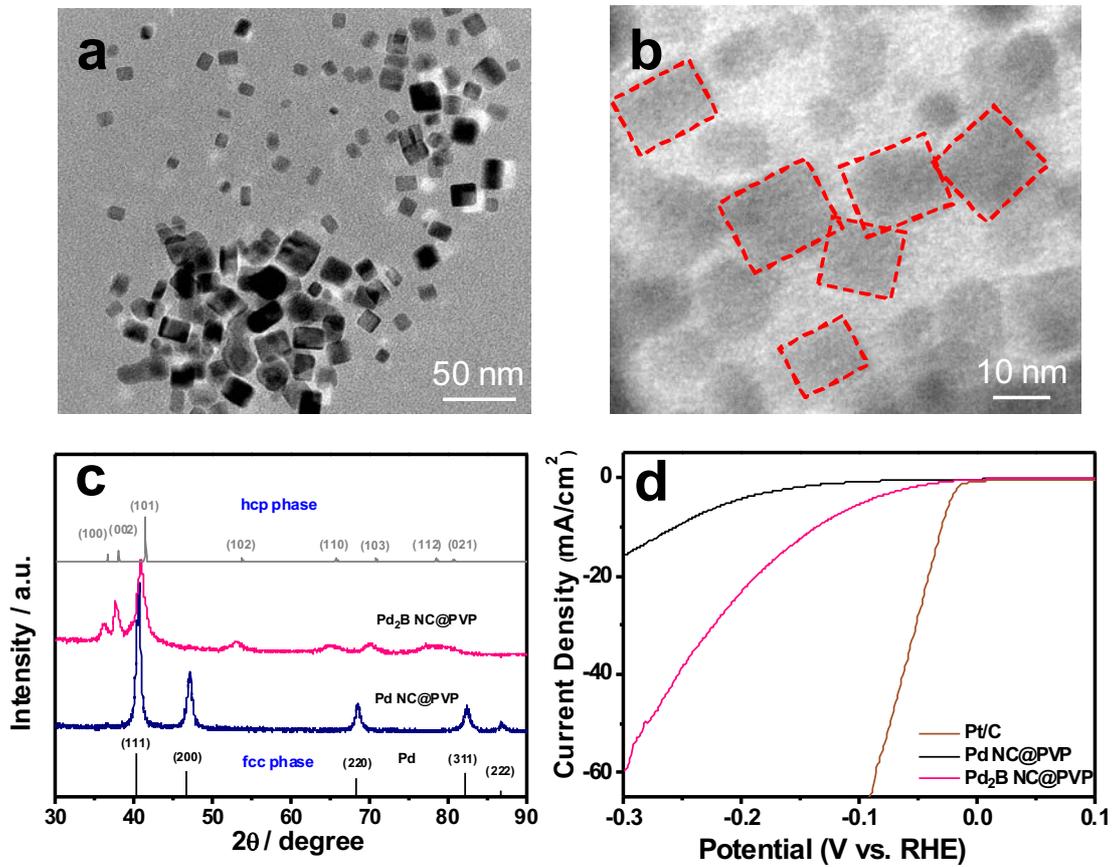
Fig. S2. TEM of Pd NC@PVP (a) and Pd₂B NC@PVP(b). (c) XRD patterns of Pd NC@PVP and Pd₂B NC@PVP. (d) Polarization curves of Pd NC@PVP, Pd₂B NC@PVP and commercial Pt/C in 0.5 M H_2SO_4 at a scan rate of 1 mV s⁻¹.

4. The SEM, TEM and EDX spectrum of the Pd₂B/C

Element	Wt %	Atomic %
B K	4.19	12.49
Pd L	70.5	21.33
C K	22.88	61.30
O K	2.43	4.88
Total:	100.00	100.00
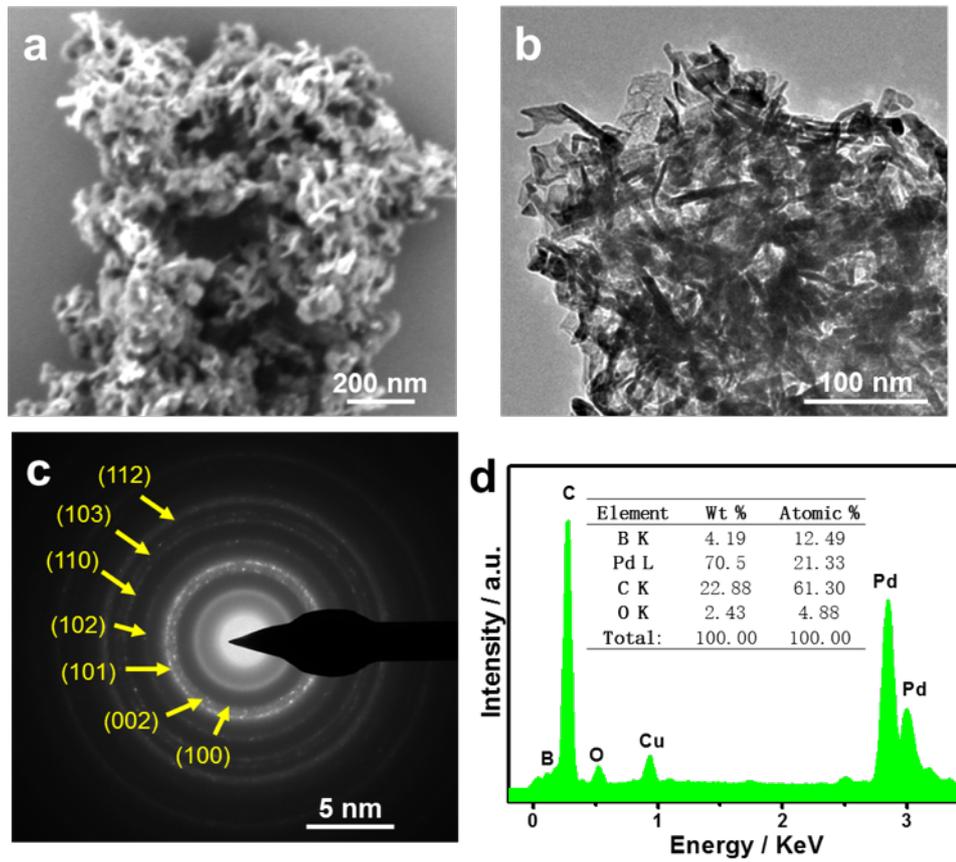
Fig. S3. (a)SEM, (b) TEM, (c) electron diffraction pattern images and (d) EDX patterns of the Pd₂B/C. The Part of C and all of O and Cu are from the carbon-coated copper grids used for TEM characterization. Insets show the atomic and weight ratios of Pd to B.

5. Table S1. EDX and ICP-MS results of Pd_xB NS/C

Catalysts	ICP-MS	EDX		Pd:B	Pd Loading
	Pd (Wt%)	Pd (Atomic %)	B (Atomic %)		on GCE /µg
Pd NS/C	42.7	28.0	0.0	-	2.14
Pd_xB NS/C(70 ^{o}C)	40.5	26.6	5.6	4.8	2.11
Pd_xB NS/C(90 ^{o}C)	39.5	21.3	5.8	3.7	1.99
Pd_2B NS/C120 ^{o}C)	34.1	21.3	12.5	1.7	1.70

6. The magnetic susceptibility of Pd and Pd$_x$B composites
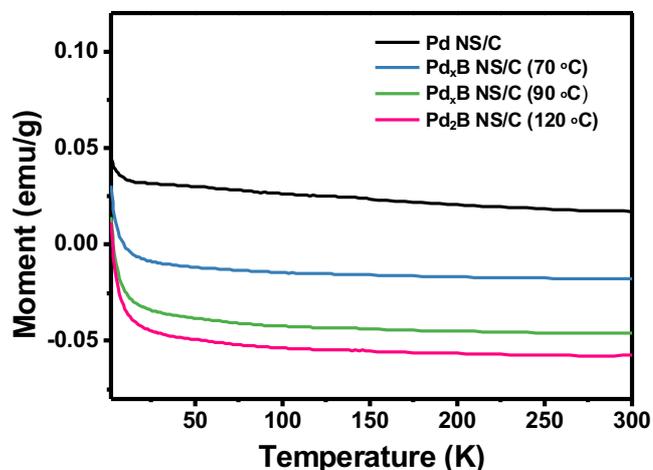
Fig. S4. Temperature dependence of the magnetic susceptibility of Pd NS and different Pd$_x$B NS/C samples synthesized at 70 ^{o}C, 90 ^{o}C and 120 ^{o}C, respectively.

The electronic structure of the Pd$_x$B samples have also been characterized by using magnetic susceptibility. The magnetic susceptibility of all Pd$_x$B samples are measured in the temperature interval between 300 and 2 K in a magnetic field of 1 T, as displayed in Figure S4. We found that with the increase of B content, the susceptibility drops sharply. While pure Pd metal has a large magnetic susceptibility due to free d electrons, the Pd$_2$B (120 ^{o}C sample) transforms largely to a diamagnetic magnetization material. This suggests that Pd forms strong covalent bonding with B that leads to the low susceptibility of d magnetism under magnetic field[1]. Our DFT calculations also confirm that with the increase of B, the d states of Pd shifts down in energy and the density of d states at the Fermi level reduces gradually.

7. DOS and UPS spectra of Pd and Pd$_x$B composites
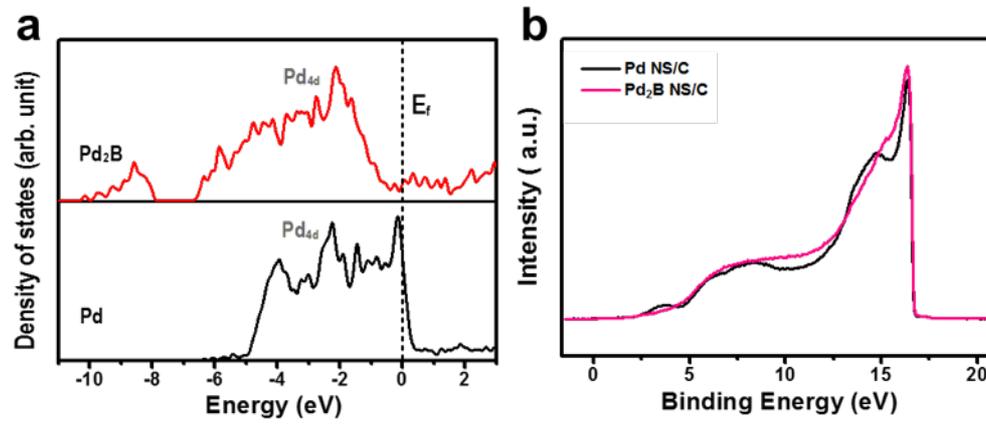
Fig. S5. (a) Density of states (DOS) of Pd and Pd$_2$B. (b) UPS spectra of Pd NS/C and Pd$_2$B NS/C.

8. XPS spectra of Pd and Pd_xB composites
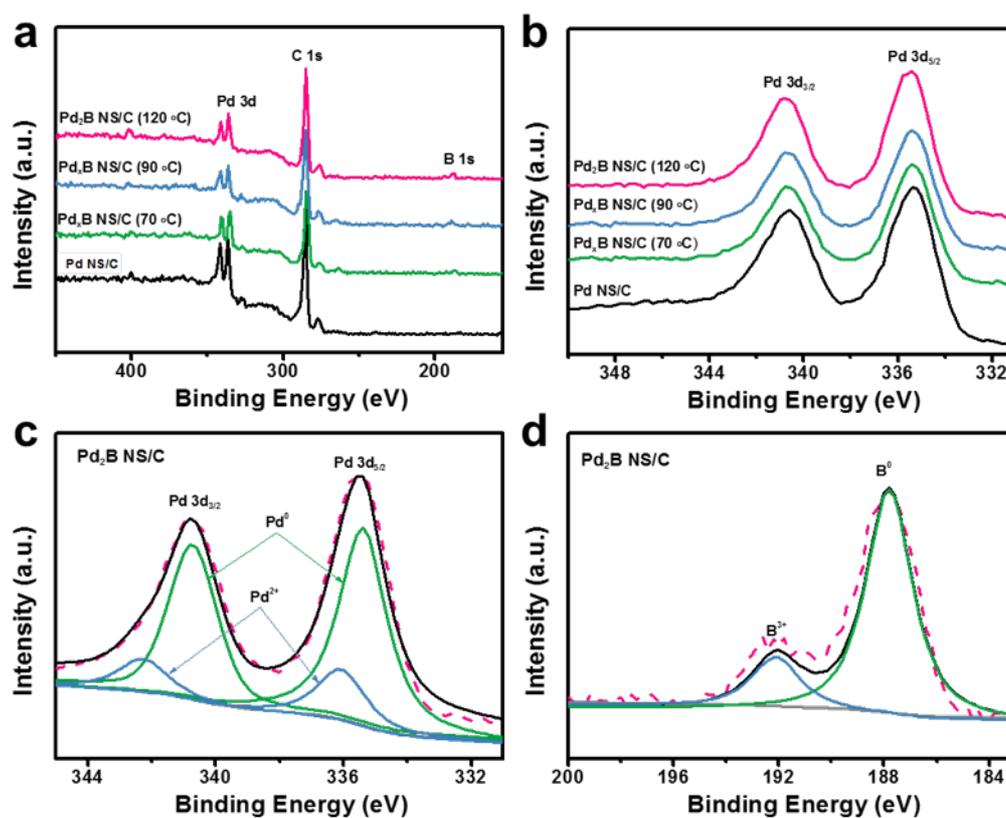
Fig. S6. (a) The survey XPS spectra of Pd and Pd_xB composites. (b) High-resolution Pd 3d of Pd and Pd_xB composites. (c) Pd 3d and (d) B 1s of Pd_2B NS/C XPS spectra. Dotted line is the experimental data, and solid lines represent fitted curve.

9. Reference electrode calibration

SCE was used as the reference electrode in all measurements and all potentials were calibrated *vs* reversible hydrogen electrode (RHE). The calibration was performed in 0.5 M H_2SO_4 bubbled with H_2 for at least 30 min. where Pt grid and carbon rod were separately used as the working and the counter electrode. SCE to be calibrated is used as a reference electrode. The potential was scanned from -0.28 to -0.2 V *vs* SCE at a scan rate of 1 mV s^{-1} and the LSV was recorded as Figure S6. The current value of 0 mA was found at -0.255 V vs. SCE for the hydrogen evolution (H^+/H_2).

The RHE potential was calculated as: E (V vs. RHE) = E (V vs. SCE) + 0.255 V.
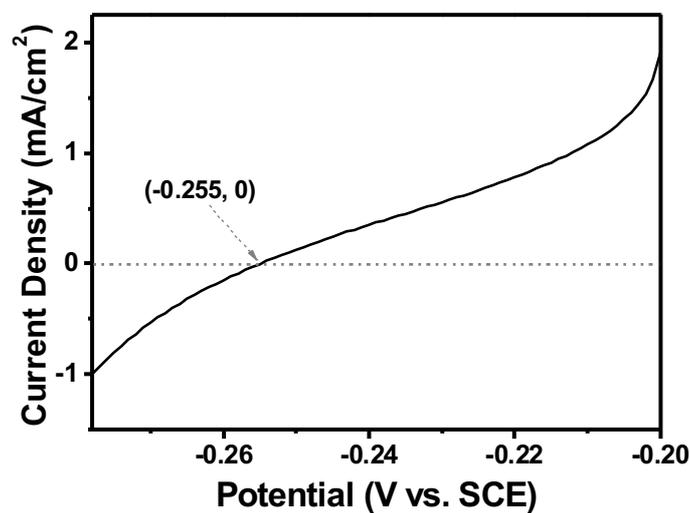
Fig. S7. Calibration of SCE in H_2 saturated 0.5 M H_2SO_4.

10. Electrochemical surface area test.
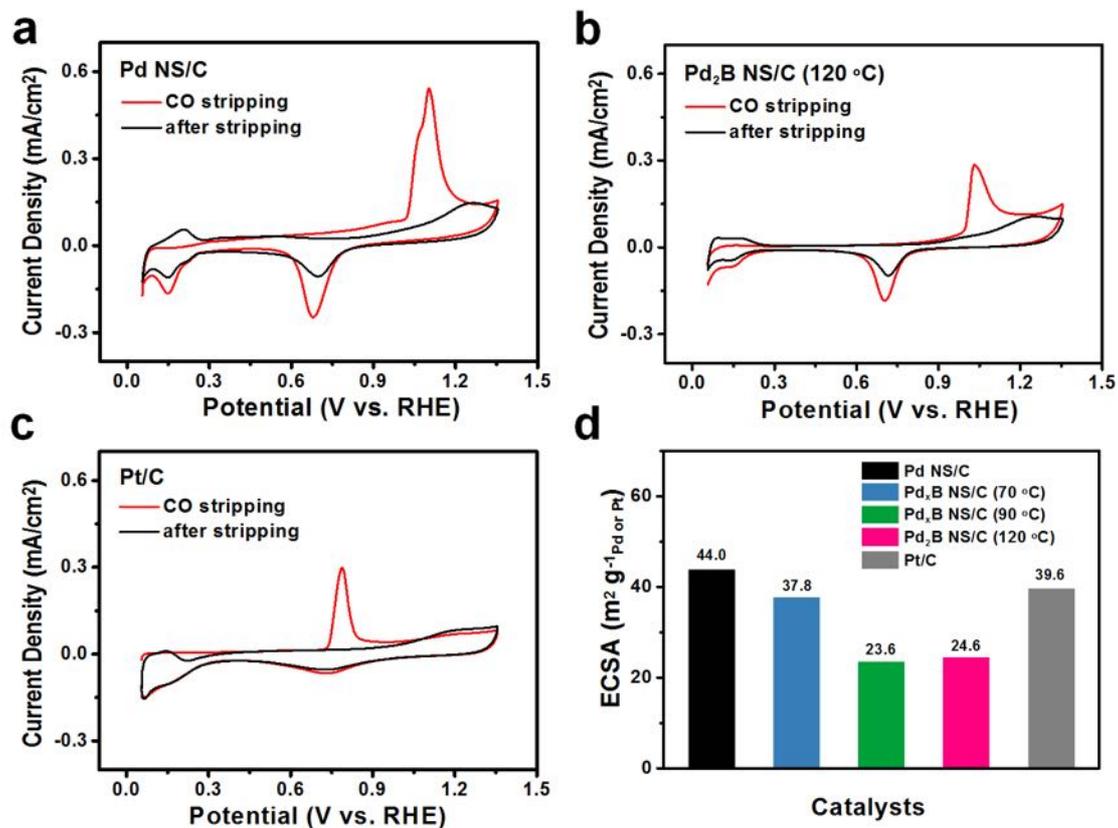
Fig. S8. CO stripping measurements of (a) Pd NS/C, (b) Pd$_2$B NS/C, (c) Pt/C in 0.5 M H$_2$SO$_4$ at a scan rate of 10 mV s^{-1}, (d) the corresponding ECSA.

11. Table S2. Summary of some recently reported representative HER electrocatalysts in acidic electrolytes (0.5 M H_2SO_4).

Catalysts	Overpotential at $j = 1$ mA cm^{-2} (mV)	Overpotential at $j = 10$ mA cm^{-2} (mV)	Tafel slope (mV dec^{-1})
Pd$_2$B/C (this work)	1.3	15.3	22.5
Ru/CN[15]	9.5	22.0	30
Au@PdAg/NRB[16]	2.0	26.2	30
PtRu@RFCS[17]	2.3	19.7	27.2
Pd/Cu-Pt/NRs[18]	-	22.8	25
400-SWNT/Pt[19]	0	27.0	38

12. The overpotentials of Pd$_x$B and Pt/C
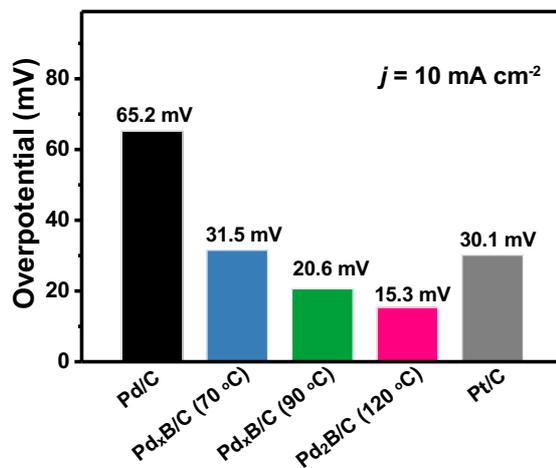
Fig. S9. Comparison of HER on Pd NS/C, Pd$_x$B NS/C (70 °C), Pd$_x$B NS/C (90 °C), Pd$_2$B NS/C (120 °C) and (e) Pt/C (20%) in acidic solutions for the overpotentials.

13. The exchange current densities of Pd_xB and Pt/C
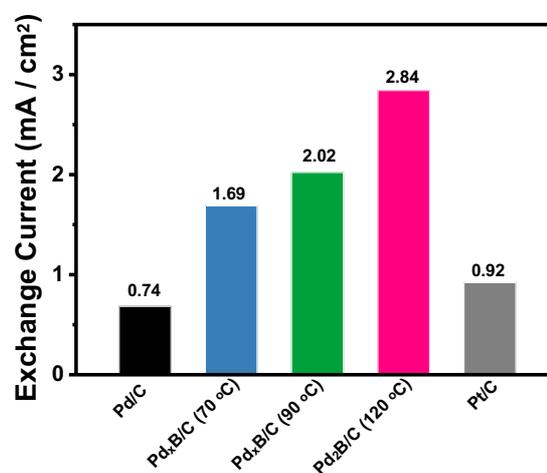
Fig. S10. Comparison of HER on Pd NS/C, Pd_xB NS/C (70 °C), Pd_xB NS/C (90 °C), Pd_2B NS/C (120 °C) and (e) Pt/C (20%) in acidic solutions for the exchange current density j_o obtained from the Butler–Volmer fitting.

14. XRD patterns of Pd₂B NS/C after stability test.
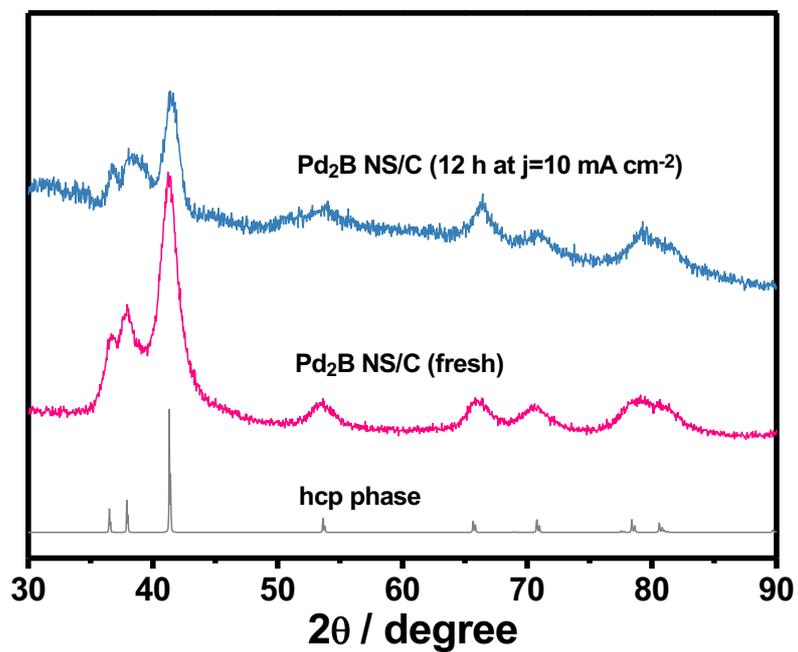
Fig. S11. XRD pattern of Pd₂B NS/C, before and after i-t test.

15. Durability measurements of the Pd$_2$B NS/C
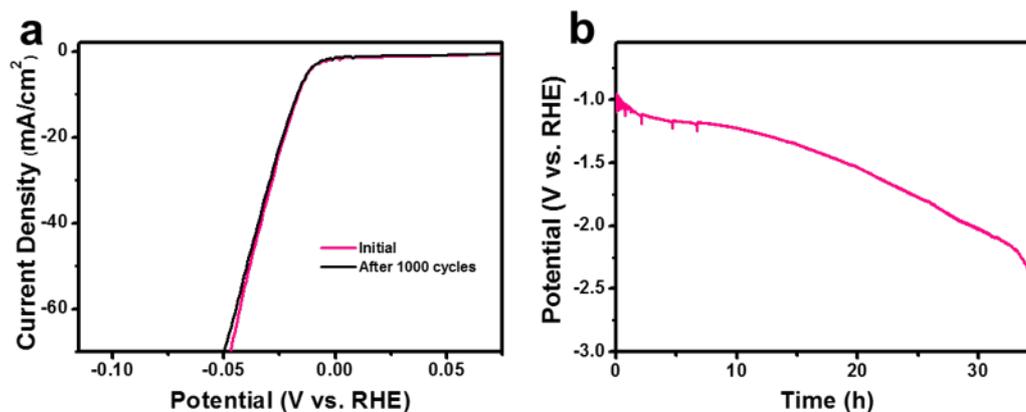
Fig. S12. Durability measurement of the Pd$_2$B NS/C. (a) The polarization curves were recorded initially and after 1,000 cyclic in 0.5 M H$_2$SO$_4$ at a scan rate of 1 mV s^{-1}. (b) Accelerated life test in 0.5 M H$_2$SO$_4$ solution.

The above results show that the polarization curve for Pd$_2$B NS/C (Figure S12a) only shifts negligibly, implying that the catalyst is stable in the typical HER working conditions. The Accelerated life test results (Figure S12b) showed that the Pd$_2$B NS/C is stable for about 33 h under the accelerated conditions. According to the simple relationship between the electrode service life (SL) and the current density (i) (SL ~ $1/i^n$), given that n is equal to 1.7 (a typical value), the service life for Pd$_2$B NS/C with a current density of 10 mA cm^{-2} was estimated to be approximately 2.9 years.

16. Pd–H underpotential absorption
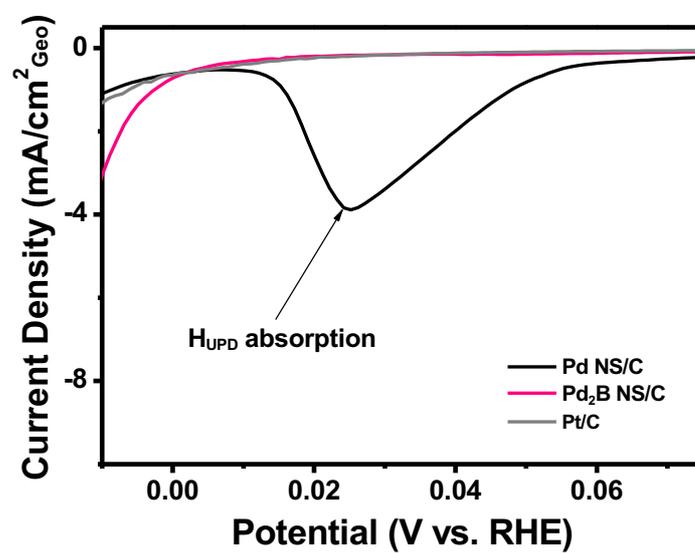
Fig. S13. Polarization curves of Pd NS and Pd$_x$B NS in 0.5 M H$_2$SO$_4$ at a scan rate of 1 mV s^{-1}.

17. DFT structures of further B diffusion without the fcc-to-hcp transition
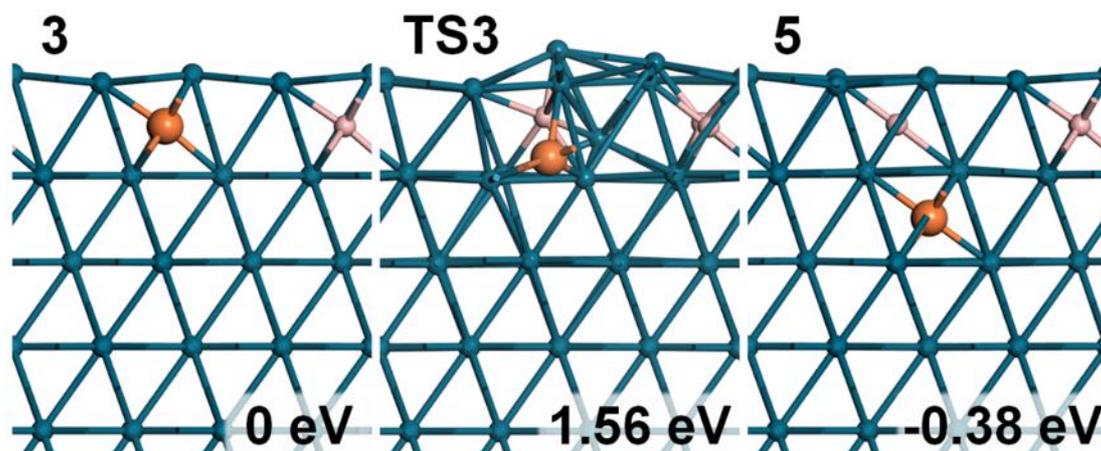
Fig. S14. The key structures of the B diffusion into the deeper bulk layers of Pd (the energetic profile is shown in Figure 3b). The initial state is the Pd (111) surface with 0.5 ML sublayer B atoms (state 3). The energies refer to state 3 were also indicated at right bottom corners.

As shown in Fig. 3b, the B diffusion from subsurface to the third sublayer is energetically exothermic by 0.38 eV. However, the reaction is highly kinetically hindered. At the transition state (TS3), the surface Pd atoms must undergo a significant reconstruction to allow the B atom to pass through the narrow T_d interstitial site, which results in a high barrier (1.56 eV).

18. H adsorption on different surface sites of Pd₂B(001).
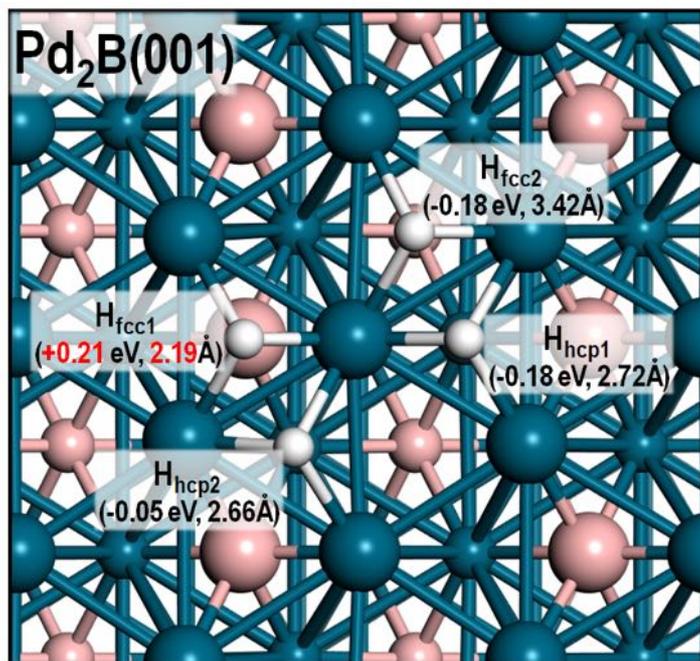
Fig. S15 The H adsorption on different surface sites of Pd$_2$B(001). The adsorption energies and the closest distances between adsorbed H and subsurface B are also labeled.

The adsorption energies of the H on most surface sites of Pd$_2$B(001) is thermodynamically exothermic (negative adsorption energy). However, the adsorption energy for the H being too close to the subsurface B (H$_{fcc1}$, sitting just above a subsurface B, with H-B distance is ~ 2.2 Å) is positive (0.21 eV). Similar trends can be found on all Pd$_x$B surfaces, which shows that a too-close contact (<2 Å) between H and B is thermodynamically prohibited.

19. XRD patterns of Pd$_2$B NS synthesized without adding amorphous Carbon.
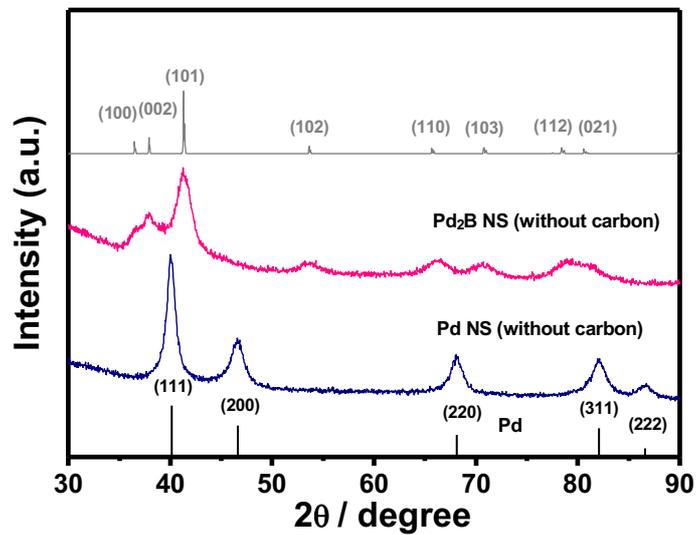
Fig. S16. XRD patterns for Pd NS and Pd$_2$B NS synthesized without adding amorphous Carbon.

References

(1)   Kobayashi, K.; Kobayashi, H.; Maesato, M.; Hayashi, M.; Yamamoto, T.; Yoshioka, S.; Matsumura, S.; Sugiyama, T.; Kawaguchi, S.; Kubota, Y.; Nakanishi, H.; Kitagawa, H. Discovery of hexagonal structured Pd-B nanocrystals. *Angew. Chem. Int. Ed.* **2017**, 56, 6578.

(2)   Hine, F.; Yasuda, M.; Noda, T.; Yoshida, T.; Okuda, J. Electrochemical Behavior of the Oxide-Coated Metal Anodes. *J. Electrochem. Soc.* **1979**, 126, 1439.

(3)   Kresse, G.; Furthmuller, J. Efficiency of ab-initio total energy calculations for metals and semiconductors using a plane-wave basis set. *Comput. Mater. Sci.* **1996**, 6, 15.

(4)   Blochl, P. E. Projector augmented-wave method. *Phys. Rev. B* **1994**, 50, 17953.

(5)   Kresse, G.; Joubert, D. From ultrasoft pseudopotentials to the projector augmented-wave method. *Phys. Rev. B* **1999**, 59, 1758.

(6)   Perdew, J. P.; Burke, K.; Ernzerhof, M. Generalized gradient approximation made simple. *Phys. Rev. Lett.* **1996**, 77, 3865.

(7)   Monkhorst, H. J.; Pack, J. D. Special points for Brillouin-zone integrations. *Phys. Rev. B* **1976**, 13, 5188.

(8)   Wang, H.-F.; Liu, Z.-P. Comprehensive mechanism and structure-sensitivity of ethanol oxidation on platinum: New transition-state searching method for resolving the complex reaction network. *J. Am. Chem. Soc.* **2008**, 130, 10996.

(9)   Shang, C.; Liu, Z.-P. Constrained Broyden minimization combined with the dimer method for locating transition state of complex reactions. *J. Chem. Theory Comput.* **2010**, 6, 1136.

(10)   Zhang, X.-J.; Shang, C.; Liu, Z.-P. Double-ended surface walking method for pathway building and transition state location of complex reactions. *J. Chem. Theory Comput.* **2013**, 9, 5745.

(11)   CRC Handbook of Chemistry and Physics; 84 ed.; R.LIDE, D., Ed.; CRC press, 2003-2004.

(12)   Liu, Z.-P.; Jenkins, S. J.; King, D. A. Car exhaust catalysis from first principles: Selective NO reduction under excess O-2 conditions on Ir. *J. Am. Chem. Soc.*, **2004**, 126, 10746-10756.

(13)   Bockris, J. O. M.; Khan, S. U. M. Surface Electrochemistry: A Molecular Level Approach, Plenum Press: New York,, 1993.

(14)   Rossmeisl, J.; Logadottir, A.; Norskov, J. K. Electrolysis of water on (oxidized) metal surfaces. *Chem. Phys.*, **2005**, 319, 178-184.

(15)   Mahmood, J.; Li, F.; Jung, S.-M.; Okyay, M. S.; Ahmad, I.; Kim, S.-J.; Park, N.; Jeong, H. Y.; Baek, J.-B. An efficient and pH-universal ruthenium-based catalyst for the hydrogen evolution reaction. *Nat. Nanotechnol.* **2017**, 12, 441.

(16)   Fan, Z.; Luo, Z.; Huang, X.; Li, B.; Chen, Y.; Wang, J.; Hu, Y.; Zhang, H. Synthesis of 4H/fcc noble multimetallic nanoribbons for electrocatalytic hydrogen evolution reaction. *J. Am. Chem. Soc.* **2016**, 138, 1414.

(17)   Li, K.; Li, Y.; Wang, Y.; Ge, J.; Liu, C.; Xing, W. Enhanced electrocatalytic performance for the hydrogen evolution reaction through surface enrichment of platinum nanoclusters alloying with ruthenium in situ embedded in carbon. *Energy Environ. Sci.* **2018**, 11, 1232.

(18)   Chao, T.; Luo, X.; Chen, W.; Jiang, B.; Ge, J.; Lin, Y.; Wu, G.; Wang, X.; Hu, Y.; Zhuang, Z.; Wu, Y.; Hong, X.; Li, Y. Atomically dispersed copper-platinum dual sites alloyed with palladium nanorings catalyze the hydrogen evolution reaction. *Angew. Chem. Int. Ed.* **2017**, 56, 16047.

(19)   Tavakkoli, M.; Holmberg, N.; Kronberg, R.; Jiang, H.; Sainio, J.; Kauppinen, E. I.; Kallio, T.; Laasonen, K. Electrochemical activation of single-walled carbon nanotubes with pseudo-atomic-scale platinum for the hydrogen evolution reaction. *ACS Catal.* **2017**, 7, 3121.